Published in final edited form as:
J Chem Theory Comput. 2011 December 13; 7(12): 4038–4049. doi:10.1021/ct2003226.

Directional Dependence of Hydrogen Bonds: a Density-based Energy Decomposition Analysis and Its Implications on Force Field Development

Zhenyu Lu[1], **Nengjie Zhou**[1], **Qin Wu**[2], and **Yingkai Zhang**[1,*]

[1]Department of Chemistry, New York University, New York 10003

[2]Center for Functional Nanomaterials, Brookhaven National Laboratory, Upton, New York 11973

Abstract

One well-known shortcoming of widely-used biomolecular force fields is the description of the directional dependence of hydrogen bonding (HB). Here we aim to better understand the origin of this difficulty and thus provide some guidance for further force field development. Our theoretical approaches center on a novel density-based energy decomposition analysis (DEDA) method [J. Chem. Phys., 131, 164112 (2009)], in which the frozen density energy is variationally determined through constrained search. This unique and most significant feature of DEDA enables us to find that the frozen density interaction term is the key factor in determining the HB orientation, while the sum of polarization and charge-transfer components shows very little HB directional dependence. This new insight suggests that the difficulty for current non-polarizable force fields to describe the HB directional dependence is not due to the lack of explicit polarization or charge-transfer terms. Using the DEDA results as reference, we further demonstrate that the main failure coming from the atomic point charge model can be overcome largely by introducing extra charge sites or higher order multipole moments. Among all the electrostatic models explored, the smeared charge distributed multipole model (up to quadrupole), which also takes account of charge penetration effects, gives the best agreement with the corresponding DEDA results. Meanwhile, our results indicate that the van der Waals interaction term needs to be further improved to better model directional hydrogen bonding.

I Introduction

While molecular modeling based on molecular mechanical force fields is becoming an indispensible tool in studying structural and dynamical properties of biomolecular systems, it has long been recognized that its applicability and reliability are critically dependent on the accuracy of the employed force field.[1–5] One main concern for currently widely employed biomolecular force fields, such as CHARMM,[6] OPLS-AA,[7] and AMBER,[8,9] is the description of the directional dependence of hydrogen bonding at the receptor atom.[1,10–17] For a hydrogen bond D-H…A, this refers to the approaching direction of the hydrogen atom to the acceptor atom A in relation to the bond(s) that A has,[10,18] as illustrated in Fig. 1. Classical force fields employing atomic point charge models and Lenard-Jones potentials would lead to very different directional preferences in comparison with results from both high level quantum chemical calculations of model complexes and detailed analyses of crystal structures.[10] This inadequacy in describing HB directional dependence has been attributed as one main factor that limits the accuracy and predictive power of force fields in modeling hydrogen bonding systems,[1,10–17] including peptide

*To whom correspondence should be addressed. yingkai.zhang@nyu.edu.

conformation preference,[11,15,19] protein folding,[1,14,17] protein-protein interactions[12,13] and ligand binding specificity.[20]

Regarding the origin of hydrogen bonding directionality, it is widely believed that in addition to the electrostatics, the HB directionality also critically depends on the polarization interactions and the charge transfer from the lone pair (*n*) of the hydrogen bond acceptor to the antibonding orbital (σ^*) of the hydrogen bond donor.[1,10–17] This opinion has been well supported by molecular orbital based energy decomposition analysis (EDA) of intermolecular interactions.[18,21,22] Currently, there are in general three strategies to tackle this HB directionality problem: 1. The addition of an explicit angle-dependent hydrogen bonding term to take account of the charge transfer effect, in which new parameters can be derived from the analysis of protein structure database[12,19] or fitted to ab initio QM calculations;[16,23,24] 2. Going beyond the atomic point charge model by introducing off-center charges to mimic lone pair electrons[25–30] or employing high order distributed multipoles to better describe electrostatics;[31–33] 3. Introduction of explicit polarization with induced point dipole,[25,34–37] drude oscillator[38–43] or fluctuating charge models.[44–47] In spite of substantial efforts, it remains a significant challenge to fundamentally understand this HB directionality problem.

Energy decomposition analysis (EDA)[48–55] based on high level quantum mechanical calculations is a powerful tool to study and analyze intermolecular interactions, and has been increasingly playing an important role in force field development.[56–58] Recently we developed a novel density-based energy decomposition analysis (DEDA) method[55] for intermolecular interactions within the framework of density functional theory. In comparison with other EDA approaches, [18,21,22,48–54,59–63] which are all wave-function-based, this new DEDA method has the following two unique features: 1. It variationally calculates the total frozen density energy through constrained search; thus it enables a clean separation of the frozen density interaction energy from the density relaxation (i.e., polarization and charge transfer) contribution. 2. The charge transfer component is also calculated variationally based on the net electron flow in real space. These unique features enable the definition of each interaction component in DEDA to be more consistent with the typical physical picture employed in the classical force field description of intermolecular interactions, and thus would make DEDA potentially more appropriate and helpful for force field development. By applying this method to the formamide dimer,[55] we showed earlier that the frozen density energy term is the dominant factor in determining the angular dependence of hydrogen bonding at the acceptor atom of the carbonyl group. This finding is quite different from the popular view regarding the origin of the hydrogen bonding directionality.[1,10–17] If it were generally true, it would mean that the difficulty for current non-polarizable force fields to describe HB orientation is not due to the lack of explicit polarization or charge-transfer terms, which implicates that the problem of HB orientation specificity can be more approachable.

In this work, we have further improved the DEDA analysis protocol, and made a systematic investigation on the directional dependence of hydrogen bonds with both B3LYP-D3 and M06-2X-D3 functionals.[64–70] The performance of both functionals to describe structures and binding interaction energies for a variety of hydrogen bonding systems have been recently extensively tested and found to be excellent.[70–74] Besides the formamide dimer, we have studied the hydrogen bonding interactions between water and molecules containing *sp* nitrogen, aromatic oxygen and sp^2, sp^3 nitrogen, oxygen and sulfur. The results clearly demonstrate that the frozen density interaction is the dominant factor in determining the HB orientation, while the sum of polarization and charge-transfer components shows very little HB directional dependence. Then using the DEDA results as reference, we have examined the performance of several electrostatic and vdW interaction models, and provided guidance

for further force field development. Systematic parameterization protocols to determine parameters for more advanced electrostatic models based on QM calculations of monomers have been explored and presented, including the off-center charge model with electrostatic potential (ESP) fitting and distributed multipole model with GDMA analysis,[32,75] with or without taking account of charge penetration effects.[76–79] For the vdW interaction, we have investigated the three most commonly employed potential energy functions,[80] i.e. Lennard–Jones 12-6 (LJ 12-6), Buffered 14-7 and Buckingham potential. In the following, we first give an introduction to the theory and methodology used in the current work, and then present our results and discuss implications on further force field development.

II Theory and Methods

A. Density-based energy decomposition analysis (DEDA) method

Recently Wu *et al*[55] developed a novel purely density-based EDA method for intermolecular binding within the framework of density functional theory. Here we first briefly review this scheme. To apply it to recent DFT methods, where the vdW attraction is taken into account to some extent either by the addition of empirical terms (i.e. the DFT-D methods[66,68,81,82]) or the parameterization of the exchange-correlation functionals (such as X3LYP[83] and M06-2X functionals[69]), we lump the Pauli repulsion and the vdW attraction together to match the vdW interaction in classical force fields. Meanwhile, BSSE-corrected fragment energies and densities are employed to eliminate the basis set superposition error (BSSE) in the DEDA analysis.

Given the formation of the complex AB without distortion of the fragment geometry, as illustrated in Fig. 2, the total BSSE-corrected binding energy can be decomposed into these contributions:

$$\Delta E_{bind}^{BSSE}=E[\rho_{AB}]-E[\rho_A^0]-E[\rho_B^0]=\Delta E_{frz}+\Delta E_{pol}+\Delta E_{ct}, \quad (1)$$

where

$$\Delta E_{frz}=\Delta E_{es}+\Delta E_{vdw}=E[\rho_A^0+\rho_B^0]-E[\rho_A^0]-E[\rho_B^0], \quad (2)$$

$$\Delta E_{es}=E_{coulomb}[\rho_A^0+\rho_B^0]-E_{coulomb}[\rho_A^0]-E_{coulomb}[\rho_B^0], \quad (3)$$

$$\Delta E_{pol}=E[\rho_{AB}^{II}]-E[\rho_A^0+\rho_B^0], \quad (4)$$

$$\Delta E_{ct}=E[\rho_{AB}]-E[\rho_{AB}^{II}]. \quad (5)$$

$E[\rho_{AB}]$ is the total energy of the binding complex AB, while $E[\rho_A^0]$ and $E[\rho_B^0]$ are total energies of non-interacting molecules A and B. They are determined with standard DFT calculations in which the energy and density for each non-interacting fragment is calculated with all basis functions in the complex as done in the standard counterpoise method.[84]

As illustrated in Fig. 2, the intermediate state I is the frozen density state, whose total density should be the superposition of two fragments' densities without any distortions. In DEDA,[55] the frozen density energy $E[\rho_A^0+\rho_B^0]$ is variationally determined with a constrained search formalism,[85] i.e., $E[\rho_A^0+\rho_B^0]=\min_{\rho\to\rho_A^0+\rho_B^0} E[\rho]$. It should be noted that in other EDA approaches,[18,21,22,48–54,59–63] the Heitler-London (HL) antisymmetrization of two fragments' wave-functions has been employed to represent such a frozen density state, in which the HL wave-function is not variationally optimized and the corresponding density does not correspond to the sum of fragments' densities.[54] Thus one most significant and novel feature of DEDA is to have a variationally determined frozen density energy through constrained search, which allows a clean separation of ΔE_{frz} from the density relaxation terms (ΔE_{pol} and ΔE_{ct}). As shown in Eq. 2 and 3, ΔE_{frz} can be further decomposed into electrostatic and vdW interaction energies, ΔE_{es} and ΔE_{vdw}, which can be served as the reference to assess the performances of electrostatic and vdW interaction models, respectively. Dispersion interactions are not explicitly included in most DFT functionals, whose performance to describe mid-range interactions can be strongly affected by the tail region of functionals[86] due to density overlap. Two recent developments to mitigate this deficiency within the GGA and hybrid functionals are: 1. adding an empirical term to model dispersion interactions (i.e. DFT-D method[66,81,82]); 2. taking the vdW interactions into account in the parameterization of the exchange-correlation functionals (such as for X3LYP[83] and M06-2X functionals[69]). For both DFT approaches, the resulting ΔE_{vdw} term in Eq. 2 would include both Pauli repulsion and vdW attraction contributions.

In order to determine ΔE_{pol} and ΔE_{ct} in Eq. 4 and 5, the total energy for a second intermediate state $E[\rho_{AB}^{II}]$ is variationally calculated, in which the molecular density is relaxed without charge transfer using the constrained DFT method.[87] ΔE_{pol} accounts for the mutual polarization effect between the fragments, and ΔE_{ct} is the contribution to the total binding energy due to the charge transfer effect between the fragments. In DEDA,[55] these two components are calculated based on density deformation and net electron flow in real space respectively, and thus show a small basis set dependence. Furthermore, the above two unique features of DEDA[55] also make the resulting frozen energy and polarization components much less affected by the inherent delocalization error[88] (i.e. the enlarged self-interaction error for a fractional number of electrons[89]) inherent in most density functionals.

B. Electrostatic Models and Parameterization Protocols

With the DEDA results as references, we have examined the performance of several electrostatic models, including point charge, off-center charge[25–30] and distributed multipole models.[31–33] The electrostatic potential (ESP) fitting method[90] has been employed to determine charge values for point charge and off-center charge models.

For the off-center charge model, extra point charges are placed on bond middle points and along the lone pair (LP) directions (see scheme 1). We have found that adding extra charge sites at bond middle points improves the description of the directional dependence of hydrogen bonding. Determining the locations of LP charges is not trivial and the optimal locations may vary with atom types.[27,28] We have tried placing the LP charges either 0.35 Å[26] or 0.74 Å[30] away from the corresponding nuclei, and found that 0.74 Å in general leads to better agreement with the DEDA results and more meaningful point charge values. Therefore, only the results of 0.74 Å are presented.

To avoid unphysical charge values due to the ill-conditioning problem of the ESP charge fit, we employed the restrained electrostatic potential (RESP) fit by adding a hyperbolic penalty function to the least squares sum,[91]

$$\chi^2=\chi^2_{esp}+\chi^2_{rest} =\sum_i\left(V_i-\widehat{V}_i\right)^2+a\sum_j\left(\left(q_j^2+b^2\right)^{1/2}-b\right), \quad (6)$$

where V_i and $\hat{V}_i$ are the electrostatic potentials calculated by quantum mechanics and the off-center atomic model at grid i, q_j is the point charge at charge site j. Parameters a = 0.005 au and b = 0.1 define the strength of the restraint and the tightness of the hyperbola around the minimum respectively. [91]

For distributed multipole models,[31–33] we have tested multipole moments up to quadrupole and the results confirm that quadrupole is necessary to yield an accurate description of the intermolecular electrostatics for HB complexes. In comparison with the distributed multipole model employed in the AMOEBA force field,[4,33,92] we also added distributed multipoles at bond middle points, which slightly improves the results. The distribute multipoles were calculated with the GDMA program version 2.2,[75] using the formatted checkpoint file produced by Gaussian03[93] as input. All distributed multipole analyses except for the furan molecule were performed with the analytical DMA algorithm by setting keywords “SWITCH 0” and “Radius H 0.35”. For the furan molecule, the analytical DMA algorithm breaks down due to a known stability problem with large basis sets.[75] Therefore, numerical DMA was performed for the furan molecule with the default setting in the program. In agreement with a previous study,[78] we find that the analytical DMA algorithm in general yields more accurate results on electrostatic potentials and intermolecular electrostatic interactions than numerical DMA.

Charge penetration[76–79] has been known to make significant contribution to intermolecular electrostatic interaction in the short range. In order to examine its effect on the description of the directional dependence of hydrogen bonding, we have replaced each point charge with a smeared charge, which consists of a nuclear charge Z and an exponential charge density $\rho(r)=\frac{qa^3}{8\pi}e^{-ar}$, in which r is the distance to the charge center and a defines the width of the charge distribution. Accordingly, the electrostatic interaction between two smeared charges can be written as:

$$E^{chg-chg}=\frac{q_Aq_B}{R}[1-f(a,b,R)-f(b,a,R)]+\frac{q_AZ_B}{R}g(a,R)+\frac{q_BZ_A}{R}g(b,R)+\frac{Z_AZ_B}{R}, \quad (7)$$

where $f(a,b,R)=e^{-aR}\frac{b^4}{(b^2-a^2)^2}\left(1-\frac{2a^2}{b^2-a^2}+\frac{aR}{2}\right)$ and $g(a,R)=1-e^{-aR}\left(1+\frac{aR}{2}\right)$.

The interaction between one smeared charge and one point dipole is

$$E^{\mathrm{chg}-dip}=-(Z_A+\lambda_3q_A)\vec{\mu}_B\cdot\frac{\vec{R}}{R^3}, \quad (8)$$

where $\lambda_3=1-e^{-aR}-a\mathrm{Re}^{-aR}-\frac{a^2R^2}{2}e^{-aR}$,

and the interaction between one smeared charge and one traceless point quadrupole is

$$E^{chg-quadrupole}=(Z_A+\lambda_5 q_4)\sum \Theta^B_{\alpha\beta}\frac{R_\alpha R_\beta}{R^5}, \tag{9}$$

where $\lambda_5=\lambda_3-\frac{1}{6}a^3R^3e^{-aR}$, and $\Theta^B_{\alpha\beta}$ is the traceless quadrupole moment at site *B*.

For each atomic center, the nuclear charge Z_A is taken as the number of valence electrons, for example $Z=4$ for the carbon atom. Parameter a for each charge site is determined by minimizing the electrostatic potential difference between quantum mechanical calculations and the damped multipolar expansion over a set of grid points.[78] The minimization is performed with the modified "potential" subprogram in TINKER 5.0.[94] The fitting grid consists of 10 layers with a spacing of 0.25 Å. The first layer starts at the distance of half of the vdW radii[95] to the atomic center.

C. VDW Interaction Models

For vdW interactions, we have investigated the three most commonly employed potential energy functions,[80] i.e. Lennard–Jones 12-6 (LJ 12-6), Buckingham and Buffered 14-7 potentials:

$$E^{IJ}_{ij}=\varepsilon_{ij}\left(\frac{R^{12}_{\min,ij}}{R^{12}_{ij}}-\frac{2R^6_{\min,ij}}{R^6_{ij}}\right), \tag{10}$$

$$E^{Buck}_{ij}=\varepsilon_{ij}\left(Ae^{-B\frac{R_{ij}}{R_{\min,ij}}}-C\frac{R^6_{\min,ij}}{R^6_{ij}}\right), \tag{11}$$

and

$$E^{buff}_{ij}=\varepsilon_{ij}\left(\frac{1+\delta}{\rho_{ij}+\delta}\right)^7\left(\frac{1+\gamma}{\rho^7_{ij}+\gamma}-2\right). \tag{12}$$

In the above equations, R_{ij} is the distance between atoms *i* and *j*, ε_{ij} is the potential well depth, $R_{\min,ij}$ is the minimum energy distance, and $\rho_{ij}=\frac{R_{ij}}{R_{\min,ij}}$ in Eq. 12. The combination rules for Eqs 10 and 11 are

$$R_{\min,ij}=r^0_i+r^0_j \text{ and } \varepsilon_{ij}=\sqrt{\varepsilon^0_i\varepsilon^0_j}. \tag{13}$$

For Eq. 12, it is

$$R_{\min,ij}=2\frac{\left(r_i^0\right)^3+\left(r_j^0\right)^3}{\left(r_i^0\right)^2+\left(r_j^0\right)^2} \text{ and } \varepsilon_{ij}=\frac{4\varepsilon_i^0\varepsilon_j^0}{\left(\left(\varepsilon_i^0\right)^{1/2}+\left(\varepsilon_j^0\right)^{1/2}\right)^2}, \quad (14)$$

where r_i^0 and ε_i^0 are vdW parameters for the atom *i*.

While Eq. 10 (LJ 12-6) is the most popular functional form for vdW interactions, Eq. 11 (Buckingham) and Eq. 12 (Buffered 14-7) are used in MM3[24] and AMOEBA[33] force fields, respectively. Following the referenced force fields,[24,33] we took A=18400.0, B=12 and C=2.25 in Eq. 11, and δ = 0.07 and γ = 0.12 in Eq. 12. r_i^0 and ε_i^0 depend on functional forms and were taken directly from the corresponding force field (OPLS-AA for LJ 12-6, MM3 for Buckingham, and AMOEBA for Buffered 14-7).

III. Computational Details

A. Hydrogen-Bond Complexes

The HB complexes investigated in this work are illustrated in Scheme 2. Except for the formamide dimer, which was shown to be representative of hydrogen bonds found in protein side chains and main chains,[10] all other complexes have water as the HB donor. The HB acceptors, as shown in scheme 1, represent a set of molecules containing *sp* nitrogen, aromatic oxygen and sp^2, sp^3 nitrogen, oxygen and sulfur. With the internal coordinates of monomers frozen and other HB geometric parameters held fixed at the optimized dimer values, we scanned along the chosen HB geometric parameters (denoted by Greek letters in Scheme 2) to generate hydrogen-bonded dimers for the DEDA calculations and model evaluations. The internal geometry of each fragment was optimized at the B3LYP/aug-cc-pvdz level with Gaussian 03.[93] We do not consider energy contributions from internal geometry distortions, i.e. the preparation energy.

B. DFT Calculations and EDA Analyses

DEDA were carried out at the B3LYP[65,67,81]-D3/aug-cc-pvdz level and M06-2X[69]-D3/aug-cc-pvdz level with a development version of NWCHEM.[96] The notation D3 indicates that the total binding energy and the vdW component from DEDA are corrected for each DFT functional by adding the dispersion energy calculated from the newest version of Grimme's method.[66] While the correction is significant for B3LYP, it is in general less than 0.1 kcal/mol for M06-2X. For the M06-2X calculations, the fine grid as implemented in NWCHEM is applied to reduce the integration grid errors when using meta-generalized-gradient approximation functionals.[97–99] The Beck's integration scheme[100] is used for the weighting function for charge partition.[55] To test the influence of the basis sets, calculations at the B3LYP-D3/aug-cc-pvtz level were also performed.

IV Results and Discussion

In this section we will first present the DEDA results for various HB complexes and our finding that frozen density interaction is the key factor in determining angular dependence of hydrogen bonds. Then by using the B3LYP DEDA results as reference, we will evaluate various electrostatic and vdW models in their descriptions of the directional hydrogen bonding.

A. DEDA of Hydrogen Bonding Directional Dependence

As illustrated in Fig. 2, the total hydrogen bonding interaction energy can be cleanly divided into four physically meaningful components, i.e., electrostatics, vdW, polarization and charge transfer. The sum of the electrostatics and vdW terms constitutes the frozen density interaction energy term, which in principle has already been taken into account in non-polarizable force fields; on the other hand, the polarization and charge transfer terms come from the electronic relaxation, whose explicit description by force fields needs polarizable models and other advanced treatment.

The DEDA results of the nine hydrogen bonding complexes (Scheme II) at their optimal HB configurations are presented in Table 1 and Fig. 3. We can see that among different functionals and basis sets, including B3LYP-D3/aug-cc-pvdz, B3LYP-D3/aug-cc-pvtz and M06-2X-D3/aug-ccpv-dz, the results are very consistent. At the optimal HB configuration, the electronic relaxation energy is about 20% of the total binding energy, which is certainly not negligible. Among the nine complexes, the ammonia–water complex has the largest contribution from electronic relaxation energy, which accounts for about 28% of the total HB binding energy. As to the influence of the basis set, the results from aug-cc-pvdz and aug-cc-pvtz are in close agreement with each other, indicating that DEDA is not sensitive to the size of the basis set. Binding energies from M06-2X-D3 are also in general very consistent with those from B3LYP-D3. We note that without the dispersion correction, an important ingredient of HB interaction,[71] B3LYP binding energies are about 1–2 kcal/mol weaker than those from M06-2X. The results in Table 1 and Figure 3 further confirm that the frozen density interaction plays a major role in determining the hydrogen bonding strength.

The DEDA results of the nine hydrogen bonding complexes with respect to their respective hydrogen bonding angles defined in Scheme II are presented in Fig. 4 and 5. For all nine complexes, we can clearly see that the frozen density interaction energy (red in Fig. 4) shares the same trend as the total binding energy (black), while the electronic relaxation energy (green) is quite flat along those defined angles. In fact, as shown in Fig. 5 (a), we see a strong correlation between ΔE_{frz} and ΔE_{bind} with respect to F. Moreover, the resemblance between ΔE_{frz} and ΔE_{bind} is not limited to the B3LYP-D3 functional. In Fig. 5 (b) we can see there is also a strong correlation between ΔE_{frz} and ΔE_{bind} for M06-2X-D3. The consistency of ΔE_{frz} between two different functionals is demonstrated in Fig. 5 (c), in which the linear regression yields a close-to-unity slope with R^2 nearly one and residual close to zero. Thus our DEDA results clearly show that the frozen density interaction term is the dominant factor in determining the hydrogen bonding orientation, while the sum of polarization and charge-transfer terms shows very little HB directional dependence. It should be noted that this finding is quite different from the current dominant view regarding the origin of hydrogen bonding directionality.[1,10–17]

In order to find out whether similar results can be observed with wave-function-based EDA methods, we also performed the same analysis with the wave-function based EDA, in which the Heitler-London (HL) antisymmetrization of two fragments' wave-functions has been employed to represent the frozen density state. The comparison of results between EDA and DEDA on the water dimer and the formamide dimer is presented in Fig. 6, and it shows three clear distinctions: (1) ΔE_{frz} from EDA is significantly smaller, which implies the contribution from electronic relaxation energy to ΔE_{bind} is significantly larger for EDA; (2) There is no strong correlation between ΔE_{frz} and ΔE_{bind} for EDA, which suggests that polarization and charge transfer play important roles in HB orientation based on wave-function-based EDA analysis; (3) EDA has a much larger difference of ΔE_{frz} between different DFT functionals than DEDA. These distinctions clearly demonstrate important novel features of the DEDA approach, and may lend DEDA some unique advantages for

force field development over the wave-function-based EDA methods. Specifically, our DEDA results indicate that the problem of describing HB orientation in current non-polarizable force fields is not due to the lack of explicit polarization or charge-transfer terms, but comes from deficiencies in electrostatic and vdW models. As shown in Fig. 7, both electrostatics and vdW interactions are important in determining the HB directionality and the optimal binding angle results from a balance between them. In next two subsections, using the DEDA results as reference, we will examine several electrostatic and vdW models in order to provide some guidance for further force field development.

B. Examination of Electrostatic Models

To go beyond the atomic charge model for better describing electrostatics interactions, there have been substantial efforts on developing off-center charge models,[25–30] which place extra point charges at sites other than the nuclei, and models employing higher multipole moments.[31–33,101] The details of implementation and parameterization can be quite diverse among different approaches. Here our strategy is to avoid the employment of dimerization data in parameterization; instead we derive all parameters by only using electrostatic properties of monomers. Thus our parameterization procedure can be directly applied to any molecules and the results will not be biased toward the HB complexes investigated here. As described in Section II, we use RESP fitting to derive charges for the off-center charge model, and the GDMA method[75] for distributed multipoles up to quadrupole.

We have examined the performance of various electrostatic models to describe directional hydrogen bonding. Correlations between ΔE_{es} from electrostatic models and the corresponding ΔE_{es} from B3LYP-D3/aug-cc-pvdz DEDA are shown in Fig. 8. For the atomic charge model (Fig. 8a), a slope of ~0.5 indicates a significant underestimation of electrostatic interactions in comparison with the DEDA results, and the root mean square deviation (RMSD) is quite large (3.7 kcal/mol). A more serious problem for the atomic charge model is that the electrostatic interaction curves are too flat for most of the HB complexes as shown in Figure 9, which is directly responsible for its problem of describing HB directionality. From Fig. 8 (b) and (c) we can see that the off-center charge model and the distributed multipole model make significant improvement over the atomic charge model: slopes are larger, RMSDs smaller, and R^2 values significantly close to unity. As shown in Fig. 9, ΔE_{es} from the distributed multipole model has a good agreement with the DEDA results except for a systematic shift that is largely due to the charge penetration effect.

The influence of charge penetration on the short range intermolecular electrostatic interactions is well known,[32] and has recently attracted much attention.[56,76–79,102,103] To account for the charge penetration effect, we replace each point charge with a smeared charge, which consists of a negative exponential charge density and a positive point charge at the atomic center.[56] The net effect of smeared charges increases the strength of electrostatic interactions at the short range. Here we have only considered the charge penetration effects for monopoles because it was shown that introducing higher order damping only yields minor improvement.[78] As demonstrated in Fig. 8, with the smeared charge model, the electrostatic interactions become much stronger and the RMSDs are all greatly reduced for all three models. There is an excellent agreement between the DEDA results and those from the smeared charge distributed multipole model, as indicated by the close-to-unity slope and the small RMSD in Fig. 8 (f). Meanwhile, by comparing the values of R^2 in Fig. 8 (a) and (d), we can see that incorporating the charge penetration effects alone would not be sufficient to relieve the problem of describing HB orientation in the atomic charge model. Among all models examined, Fig. 8 and 9 clearly show that the smeared charge distributed multipole model (up to quadrupole), which takes account of charge penetration effect, has the best agreement with the corresponding DEDA results.

C. Examination of vdW Models

As shown in Fig. 7, not only electrostatics, but also vdW interactions can be important in determining the HB directionality. Here we have investigated three commonly employed vdW force field functions. The vdW parameters were directly taken from OPLS-AA[7], AMOEBA[92] and MM3[24] force fields respectively to test the LJ12-6, Buffered 14-7 and Buckingham potentials. These parameters are in general obtained by fitting to experimentally measured properties or high-level *ab initio* QM calculations of dimerization energies. Thus we do not expect that the vdW function forms with parameters taken directly from those force fields have a good agreement with the DEDA results. Nevertheless, such a comparison may shed light on the appropriateness of vdW function forms to describe the angular dependence of hydrogen bonding.

The correlations between ΔE_{vdw} from vdW models and those from B3LYP-D3 DEDA are presented in Fig. 10. Among the three models, LJ 12-6 model is clearly the worst, and does not correlate at all with the corresponding DEDA results. The performances of Buffered 14-7 and Buckingham potentials are comparable. Both models have some weak correlations with the DEDA results, but are still not satisfactory in describing the angular dependency of vdW interaction, as shown in Fig. 11. To significantly improve the description of vdW interactions, a systematic parameterization protocol should be developed and more advanced vdw models may also need to be explored. We are currently carrying out studies along this direction and will present our results in future account.

V Conclusions

In this work, we have further improved the density-based energy decomposition analysis (DEDA) method, and made a systematic investigation about the directional dependence hydrogen bonding with both B3LYP-D3 and M06-2X-D3 functionals. Our results clearly demonstrate that frozen density interaction energy term is the key factor in determining the HB orientation, while the density relaxation energy, including both polarization and charge-transfer components, shows very little HB directional dependence. This finding is quite different from the current dominant view regarding the origin of hydrogen bonding directionality, and would not be obtained with wave-function-based EDA approaches. Using the DEDA results as reference, we have examined several electrostatic and vdW interaction models, and demonstrated that the main deficiency coming from the atomic point charge model can be overcome largely by the introduction of extra charge sites or higher order multipole moments. Among all electrostatic models explored, the smeared charge distributed multipole model (up to quadrupole) is found to have the best agreement with the corresponding DEDA results. Systematic parameterization protocols to determine parameters for more advanced electrostatic models based on QM calculations of monomers have been presented. We have also shown that van der Waals models still need further improvement to better model the directional dependence of hydrogen bonding.

Acknowledgments

This work carried out in part at NYU was supported by NIH (R01-GM079223) and NSF-MRSEC (DMR-0820341). Research carried out in part at the Center for Functional Nanomaterials was supported by the U.S. Department of Energy, Office of Basic Energy Sciences under Contract No. DE-AC02-98CH10886. We thank NYU-ITS and CFN for providing computational resources.

References

1. Freddolino PL, Harrison CB, Liu YX, Schulten K. Nat Phys. 2010; 6:751–758. [PubMed: 21297873]
2. Jorgensen WL. Science. 2004; 303:1813–1818. [PubMed: 15031495]

3. Karplus M, McCammon JA. Nat Struct Biol. 2002; 9:646–652. [PubMed: 12198485]
4. Ponder JW, Case DA. Adv Protein Chem. 2003; 66:27. [PubMed: 14631816]
5. van Gunsteren WF, Bakowies D, Baron R, Chandrasekhar I, Christen M, Daura X, Gee P, Geerke DP, Glattli A, Hunenberger PH, Kastenholz MA, Ostenbrink C, Schenk M, Trzesniak D, van der Vegt NFA, Yu HB. Angew Chem, Int Ed. 2006; 45:4064–4092.
6. MacKerell AD, Bashford D, Bellott M, Dunbrack RL, Evanseck JD, Field MJ, Fischer S, Gao J, Guo H, Ha S, Joseph-McCarthy D, Kuchnir L, Kuczera K, Lau FTK, Mattos C, Michnick S, Ngo T, Nguyen DT, Prodhom B, Reiher WE, Roux B, Schlenkrich M, Smith JC, Stote R, Straub J, Watanabe M, Wiorkiewicz-Kuczera J, Yin D, Karplus M. J Phys Chem B. 1998; 102:3586–3616.
7. Jorgensen WL, Maxwell DS, TiradoRives J. J Am Chem Soc. 1996; 118:11225–11236.
8. Cornell WD, Cieplak P, Bayly CI, Gould IR, Merz KM, Ferguson DM, Spellmeyer DC, Fox T, Caldwell JW, Kollman PA. J Am Chem Soc. 1995; 117:5179–5197.
9. Wang JM, Cieplak P, Kollman PA. J Comput Chem. 2000; 21:1049–1074.
10. Morozov AV, Kortemme T, Tsemekhman K, Baker D. Proc Natl Acad Sci U S A. 2004; 101:6946–6951. [PubMed: 15118103]
11. Best RB, Hummer G. J Phys Chem B. 2009; 113:9004–9015. [PubMed: 19514729]
12. Kortemme T, Morozov AV, Baker D. J Mol Biol. 2003; 326:1239–1259. [PubMed: 12589766]
13. Choi H, Kang H, Park H. J Phys Chem B. 2010; 114:2980–2987. [PubMed: 20141111]
14. Day R, Paschek D, Garcia AE. Proteins: Struct, Funct, Bioinf. 2010; 78:1889–1899.
15. Cao ZX, Lin ZX, Wang J, Liu HY. J Comput Chem. 2009; 30:645–660. [PubMed: 18780355]
16. Lii JH, Allinger NL. J Phys Chem A. 2008; 112:11903–11913. [PubMed: 18942820]
17. Freddolino PL, Park S, Roux B, Schulten K. Biophys J. 2009; 96:3772–3780. [PubMed: 19413983]
18. Umeyama H, Morokuma K. J Am Chem Soc. 1977; 99:1316–1332.
19. Grishaev A, Bax A. J Am Chem Soc. 2004; 126:7281–7292. [PubMed: 15186165]
20. Bissantz C, Kuhn B, Stahl M. J Med Chem. 2010; 53:5061–5084. [PubMed: 20345171]
21. Khaliullin RZ, Cobar EA, Lochan RC, Bell AT, Head-Gordon M. J Phys Chem A. 2007; 111:8753–8765. [PubMed: 17655284]
22. Chen W, Gordon MS. J Phys Chem. 1996; 100:14316–14328.
23. Choi H, Kang H, Park H. J Comput Chem. 2010; 31:897–903. [PubMed: 19618414]
24. Allinger NL, Yuh YH, Lii JH. J Am Chem Soc. 1989; 111:8551–8566.
25. Cieplak P, Caldwell J, Kollman P. J Comput Chem. 2001; 22:1048–1057.
26. Dixon RW, Kollman PA. J Comput Chem. 1997; 18:1632–1646.
27. Karamertzanis PG, Pantelides CC. Mol Simul. 2004; 30:413–436.
28. Tschampel SM, Kennerty MR, Woods R. J J Chem Theory Comput. 2007; 3:1721–1733.
29. Wang ZX, Zhang W, Wu C, Lei HX, Cieplak P, Duan Y. J Comput Chem. 2006; 27:781–790. [PubMed: 16526038]
30. Zhao DX, Liu C, Wang FF, Yu CY, Gong LD, Liu SB, Yang ZZ. J Chem Theory Comput. 2010; 6:795–804.
31. Buckingham AD, Fowler PW. Can J Chem. 1985; 63:2018–2025.
32. Stone, AJ. The theory of intermolecular forces. Clarendon Press; Oxford University Press; Oxford Oxford; New York: 1996.
33. Ren PY, Ponder JW. J Phys Chem B. 2003; 107:5933–5947.
34. Warshel A, Levitt M. J Mol Biol. 1976; 103:227–249. [PubMed: 985660]
35. Ren PY, Ponder JW. J Comput Chem. 2002; 23:1497–1506. [PubMed: 12395419]
36. Xie WS, Pu JZ, MacKerell AD, Gao JL. J Chem Theory Comput. 2007; 3:1878–1889. [PubMed: 18958290]
37. Thole BT. Chem Phys. 1981; 59:341–350.
38. Sprik M, Klein ML. J Chem Phys. 1988; 89:7556–7560.
39. Straatsma TP, Mccammon JA. Chem Phys Lett. 1990; 167:252–254.
40. van Maaren PJ, van der Spoel D. J Phys Chem B. 2001; 105:2618–2626.

41. Lamoureux G, Roux BJ. Chem Phys. 2003; 119:3025–3039.
42. Yu HB, Hansson T, van Gunsteren WF. J Chem Phys. 2003; 118:221–234.
43. Anisimov VM, Lamoureux G, Vorobyov IV, Huang N, Roux B, MacKerell AD. J Chem Theory Comput. 2005; 1:153–168.
44. Rappe AK, Goddard WA. J Phys Chem. 1991; 95:3358–3363.
45. Rick SW, Stuart SJ, Berne BJ. J Chem Phys. 1994; 101:6141–6156.
46. York DM, Yang WT. J Chem Phys. 1996; 104:159–172.
47. Patel S, Mackerell AD, Brooks CL. J Comput Chem. 2004; 25:1504– 1514. [PubMed: 15224394]
48. Morokuma K. J Chem Phys. 1971; 55:1236.
49. Kitaura K, Morokuma K. Int J Quantum Chem. 1976; 10:325–340.
50. Stevens WJ, Fink WH. Chem Phys Lett. 1987; 139:15–22.
51. Frey RF, Davidson ER. J Chem Phys. 1989; 90:5555–5562.
52. Bagus PS, Illas F. J Chem Phys. 1992; 96:8962–8970.
53. Mo YR, Gao JL, Peyerimhoff SD. J Chem Phys. 2000; 112:5530–5538.
54. Mitoraj MP, Michalak A, Ziegler T. J Chem Theory Comput. 2009; 5:962–975.
55. Wu Q, Ayers PW, Zhang YK. J Chem Phys. 2009; 131:164112. [PubMed: 19894932]
56. Donchev AG, Ozrin VD, Subbotin MV, Tarasov OV, Tarasov VI. Proc Natl Acad Sci U S A. 2005; 102:7829–7834. [PubMed: 15911753]
57. Piquemal JP, Chevreau H, Gresh N. J Chem Theory Comput. 2007; 3:824–837.
58. Wu JC, Piquemal JP, Chaudret R, Reinhardt P, Ren PY. J Chem Theory Comput. 2010; 6:2059–2070. [PubMed: 21116445]
59. Mayer I. Phys Chem Chem Phys. 2006; 8:4630–4646. [PubMed: 17047759]
60. Reinhardt P, Piquemal JP, Savin A. J Chem Theory Comput. 2008; 4:2020–2029.
61. Mo YR, Bao P, Gao JL. Phys Chem Chem Phys. 2011; 13:6760–6775. [PubMed: 21369567]
62. Mo YR, Song LC, Lin YC. J Phys Chem A. 2007; 111:8291–8301. [PubMed: 17655207]
63. Steinmann SN, Corminboeuf C, Wu W, Mo YR. J Phys Chem A. 2011; 115:5467–5477. [PubMed: 21557586]
64. Becke AD. Phys Rev A. 1988; 38:3098–3100. [PubMed: 9900728]
65. Becke AD. J Chem Phys. 1993; 98:5648–5652.
66. Grimme S, Antony J, Ehrlich S, Krieg H. J Chem Phys. 2010; 132:154104. [PubMed: 20423165]
67. Lee CT, Yang WT, Parr RG. Physical Review B. 1988; 37:785–789.
68. Wu Q, Yang WT. J Chem Phys. 2002; 116:515–524.
69. Zhao Y, Truhlar DG. Theor Chem Acc. 2008; 120:215–241.
70. Zhao Y, Truhlar DG. Acc Chem Res. 2008; 41:157–167. [PubMed: 18186612]
71. Thanthiriwatte KS, Hohenstein EG, Burns LA, Sherrill CD. J Chem Theory Comput. 2011; 7:88–96.
72. Hujo W, Grimme S. Phys Chem Chem Phys. 2011; 13:13942–13950. [PubMed: 21594296]
73. Riley KE, Pitonak M, Jurecka P, Hobza P. Chem Rev (Washington, DC, U S). 2010; 110:5023–5063.
74. Riley KE, Pitonak M, Cerny J, Hobza P. J Chem Theory Comput. 2010; 6:66–80.
75. Stone AJ. J Chem Theory Comput. 2005; 1:1128–1132.
76. Cisneros GA, Tholander SNI, Parisel O, Darden TA, Elking D, Perera L, Piquemal JP. Int J Quantum Chem. 2008; 108:1905–1912. [PubMed: 19606279]
77. Piquemal JP, Gresh N, Giessner-Prettre C. J Phys Chem A. 2003; 107:10353–10359.
78. Slipchenko LV, Gordon MS. J Comput Chem. 2007; 28:276–291. [PubMed: 17143863]
79. Wang B, Truhlar DG. J Chem Theory Comput. 2010; 6:3330–3342.
80. Halgren TA. J Am Chem Soc. 1992; 114:7827–7843.
81. Grimme S. J Comput Chem. 2006; 27:1787–1799. [PubMed: 16955487]
82. Jurecka P, Cerny J, Hobza P, Salahub DR. J Comput Chem. 2007; 28:555–569. [PubMed: 17186489]

83. Xu X, Goddard WA. Proc Natl Acad Sci U S A. 2004; 101:2673–2677. [PubMed: 14981235]
84. Boys SF, Bernardi F. Mol Phys. 1970; 19:553.
85. Wu Q, Yang WT. J Chem Phys. 2003; 118:2498–2509.
86. Zhang YK, Pan W, Yang WT. J Chem Phys. 1997; 107:7921–7925.
87. Wu Q, Van Voorhis T. Phys Rev A. 2005; 72
88. Cohen AJ, Mori-Sanchez P, Yang WT. Science. 2008; 321:792–794. [PubMed: 18687952]
89. Zhang YK, Yang WT. J Chem Phys. 1998; 109:2604–2608.
90. Breneman CM, Wiberg KB. J Comput Chem. 1990; 11:361–373.
91. Bayly CI, Cieplak P, Cornell WD, Kollman PA. J Phys Chem. 1993; 97:10269–10280.
92. Ponder JW, Wu CJ, Ren PY, Pande VS, Chodera JD, Schnieders MJ, Haque I, Mobley DL, Lambrecht DS, DiStasio RA, Head-Gordon M, Clark GNI, Johnson ME, Head-Gordon T. J Phys Chem B. 2010; 114:2549–2564. [PubMed: 20136072]
93. Frisch, MJ.; Trucks, GW.; Schlegel, HB.; Scuseria, GE.; Robb, MA.; Cheeseman, JRJ.; Vreven, T.; Kudin, KN.; Burant, JC.; Millam, JM.; Iyengar, SS.; Tomasi, J.; Barone, V.; Mennucci, B.; Cossi, M.; Scalmani, G.; Rega, N.; Petersson, GA.; Nakatsuji, H.; Hada, M.; Ehara, M.; Toyota, K.; Fukuda, R.; Hasegawa, J.; Ishida, M.; Nakajima, T.; Honda, Y.; Kitao, O.; Nakai, H.; Klene, M.; Li, X.; Knox, JE.; Hratchian, HP.; Cross, JB.; Adamo, C.; Jaramillo, J.; Gomperts, R.; Stratmann, RE.; Yazyev, O.; Austin, AJ.; Cammi, R.; Pomelli, C.; Ochterski, JW.; Ayala, PY.; Morokuma, K.; Voth, GA.; Salvador, P.; Dannenberg, JJ.; Zakrzewski, VG.; Dapprich, S.; Daniels, AD.; Strain, MC.; Farkas, O.; Malick, DK.; Rabuck, AD.; Raghavachari, K.; Foresman, JB.; Ortiz, JV.; Cui, Q.; Baboul, AG.; Clifford, S.; Cioslowski, J.; Stefanov, BB.; Liu, G.; Liashenko, A.; Piskorz, P.; Komaromi, I.; Martin, RL.; Fox, DJ.; Keith, T.; Al-Laham, MA.; Peng, CY.; Nanayakkara, A.; Challacombe, M.; Gill, PMW.; Johnson, B.; Chen, W.; Wong, MW.; Gonzalez, C.; Pople, JA. Gaussian 03, Revision B.05. Gaussian, Inc; Pittsburgh PA: 2003.
94. Ponder, JW. TINKER, Software Tools for Molecular Design, Version 5.0. 2009.
95. Bondi A. J Phys Chem. 1964; 68:441.
96. Kendall RA, Apra E, Bernholdt DE, Bylaska EJ, Dupuis M, Fann GI, Harrison RJ, Ju JL, Nichols JA, Nieplocha J, Straatsma TP, Windus TL, Wong AT. Comput Phys Commun. 2000; 128:260–283.
97. Johnson ER, Wolkow RA, DiLabio GA. Chem Phys Lett. 2004; 394:334–338.
98. Johnson ER, Becke AD, Sherrill CD, DiLabio GA. J Chem Phys. 2009; 131:34111.
99. Wheeler SE, Houk KN. J Chem Theory Comput. 2010; 6:395–404. [PubMed: 20305831]
100. Becke AD. J Chem Phys. 1988; 88:2547–2553.
101. Gordon MS, Freitag MA, Bandyopadhyay P, Jensen JH, Kairys V, Stevens WJ. J Phys Chem A. 2001; 105:293–307.
102. Louwen JN, Vogt ETC. J Mol Catal A: Chem. 1998; 134:63–77.
103. Elking DM, Cisneros GA, Piquemal JP, Darden TA, Pedersen LG. J Chem Theory Comput. 2010; 6:190–202. [PubMed: 20209077]

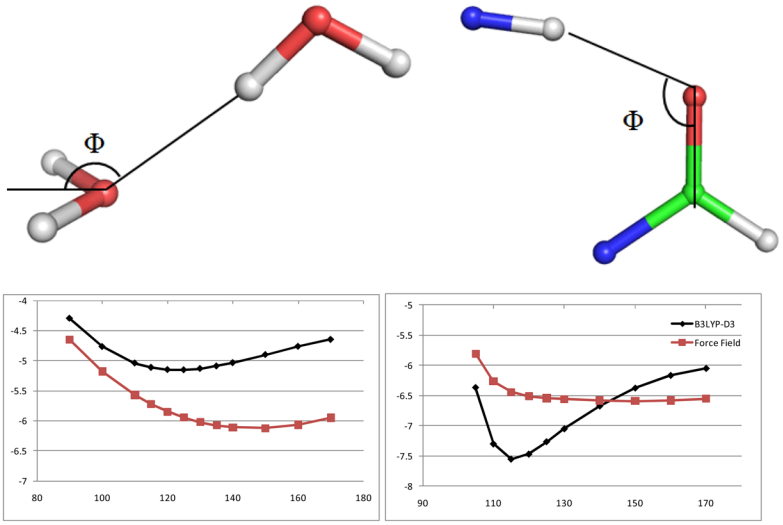

Figure 1.

Illustration of the failure of classical atomic-charge based force fields in modeling the hydrogen bonding angular depenency. Please see Ref. 10 for a more detailed discussion of this problem. Upper panel: Φ angle for water and formamide dimers; Lower panel: binding energies along the Φ angle from high level QM calculations (black) and force field calculations using atomic charge and LJ 12-6 model (Red). Energy is in kcal/mol.

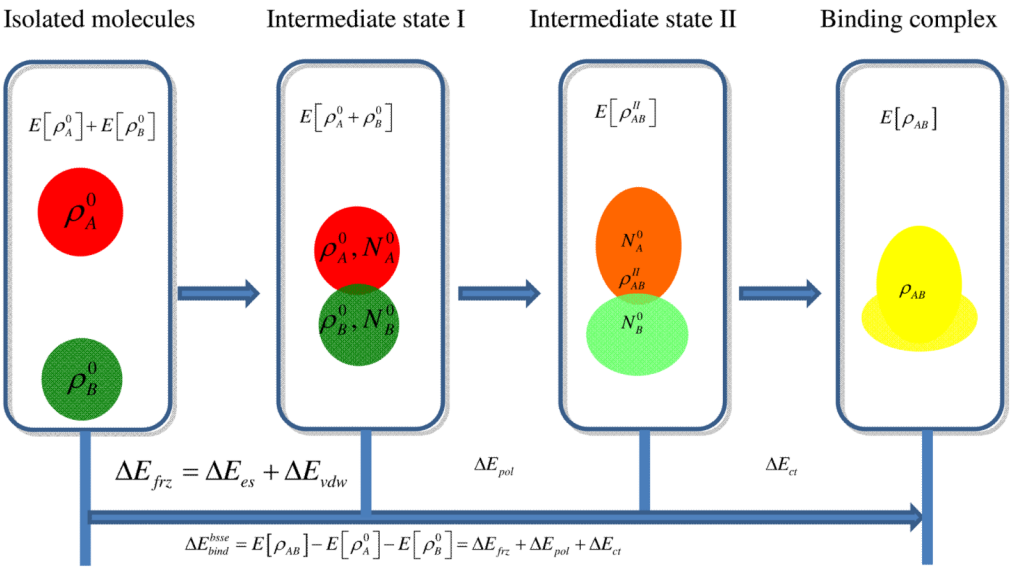

Figure 2.
Illustration of the DEDA scheme.

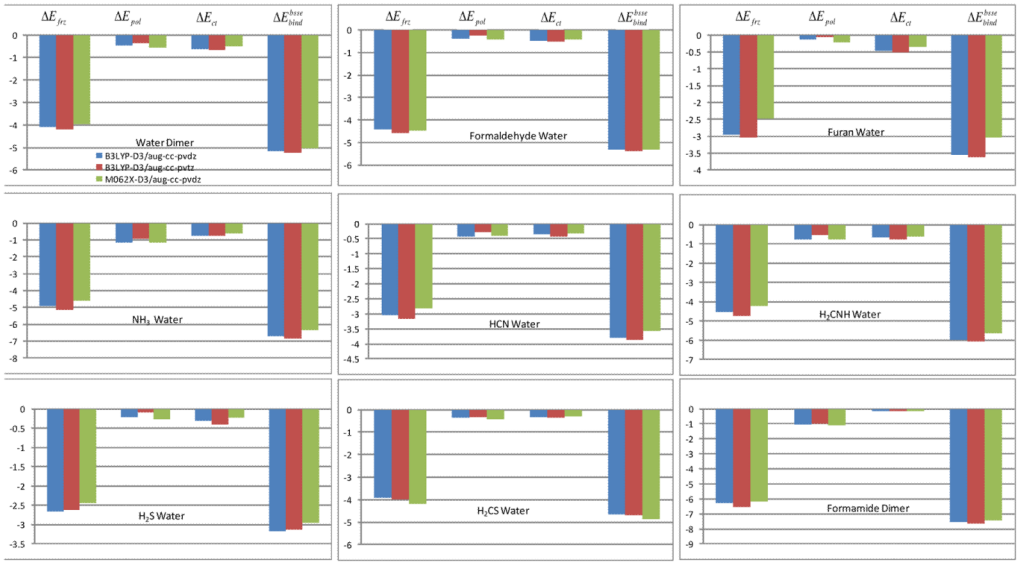

Figure 3.
Total binding energy and its components for each HB complex at geometries optimized at the B3LYP/aug-cc-pvdz level.

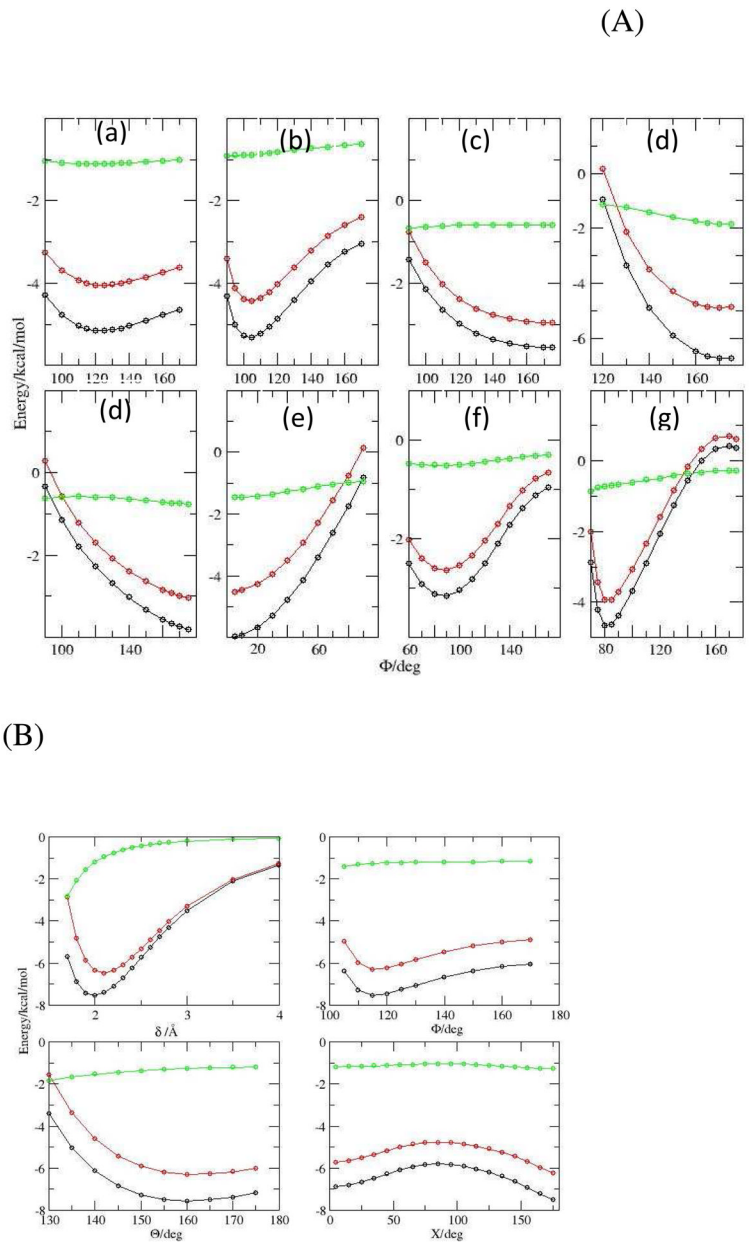

Figure 4.

Total binding energy and its components from B3LYP-D3/aug-cc-pvdz DEDA along the HB angles (see scheme 2). Black: total binding energy; Red: frozen density energy; Green: electronic relaxation energy (polarization and charge transfer). Panel A: (a) Water Dimer; (b) Formaldehyde–Water; (c) Furan–Water; (d) Ammonia–Water; (e) Hydrogen Cyanide–Water; (f) Methanimine–Water; (g) Hydrogen Sulfide–Water. Panel B: Formamide Dimer.

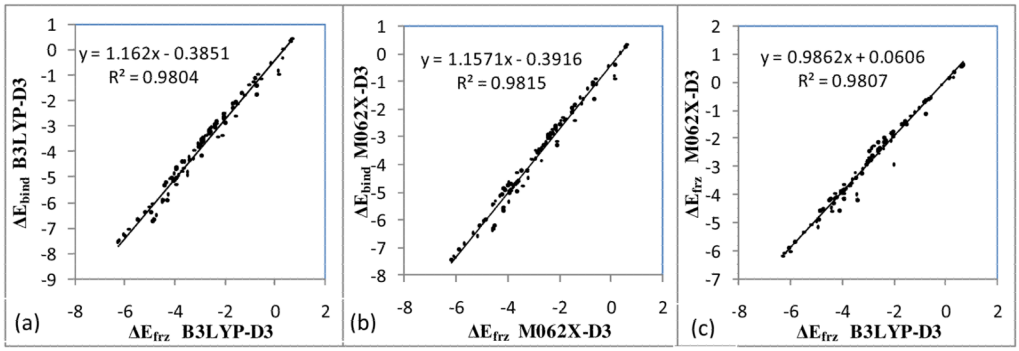

Figure 5.

Linear regressions for total binding energy and frozen density interaction results (in kcal/mol) along HB angles. (a). For B3LYP-D3, ΔE_{frz} vs. ΔE_{bind}. (b). For M06-2X-D3, ΔE_{frz} vs. ΔE_{bind}. (c) For ΔE_{frz}, B3LYP-D3 vs. M06-2X-D3.

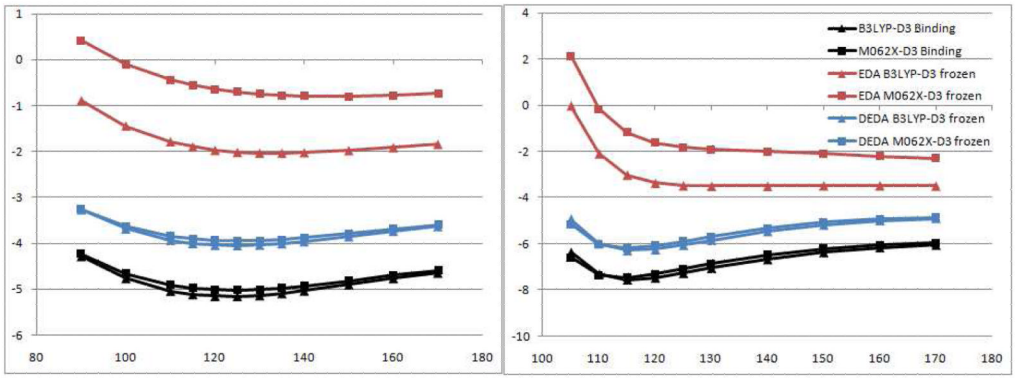

Figure 6.

Comparision of frozen energies in kcal/mol along the Φ angle (see Fig. 1) for water dimer (left) and formamide dimer (right) with DEDA and the wave-function based EDA. The latter employs the Heitler-London (HL) antisymmetrization of two fragments' wave-functions to represent the frozen density state.

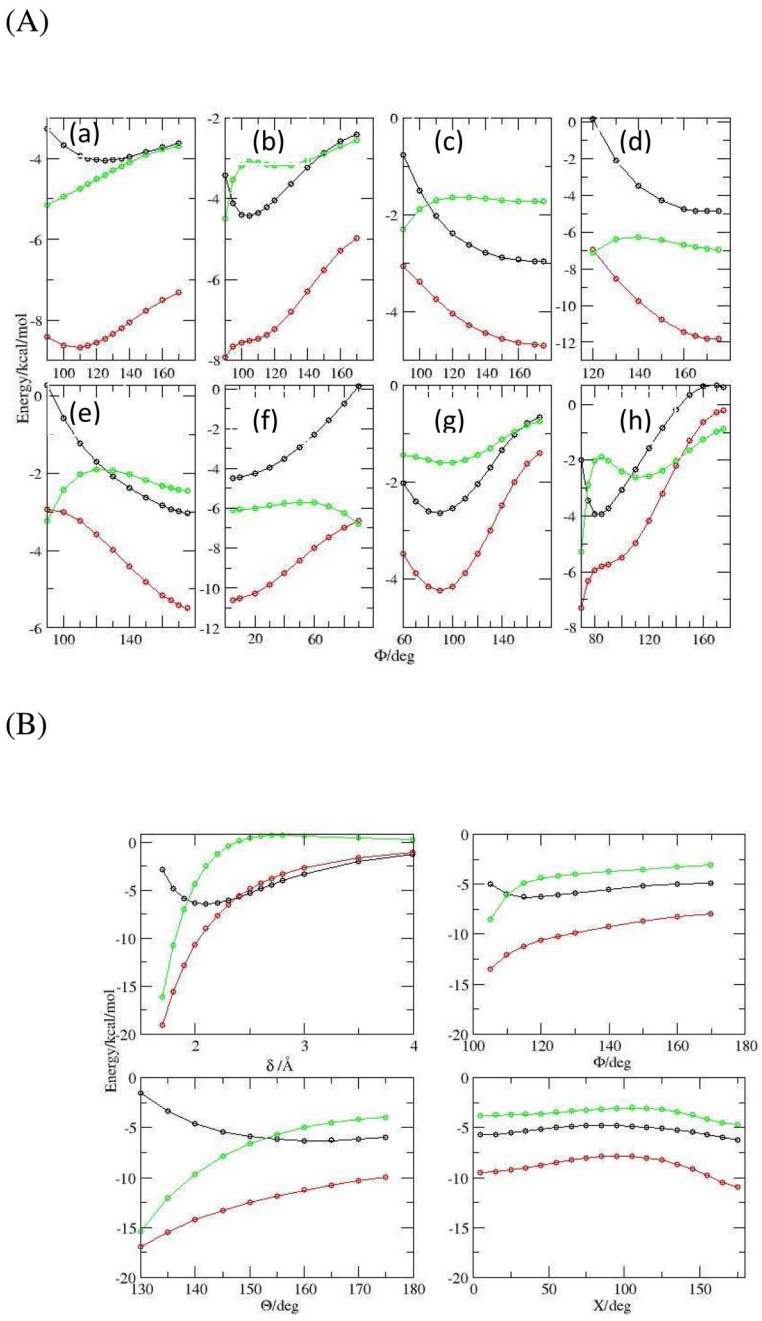

Figure 7.

Frozen density energy, electrostatics and vdW energy (in reversed sign) from B3LYP-D3 EDA along the HB angles (see scheme 2). Black: frozen density energy; Red: electrostatics; Green: vdW in reversed sign. Other descriptions are the same as those in Figure 4.

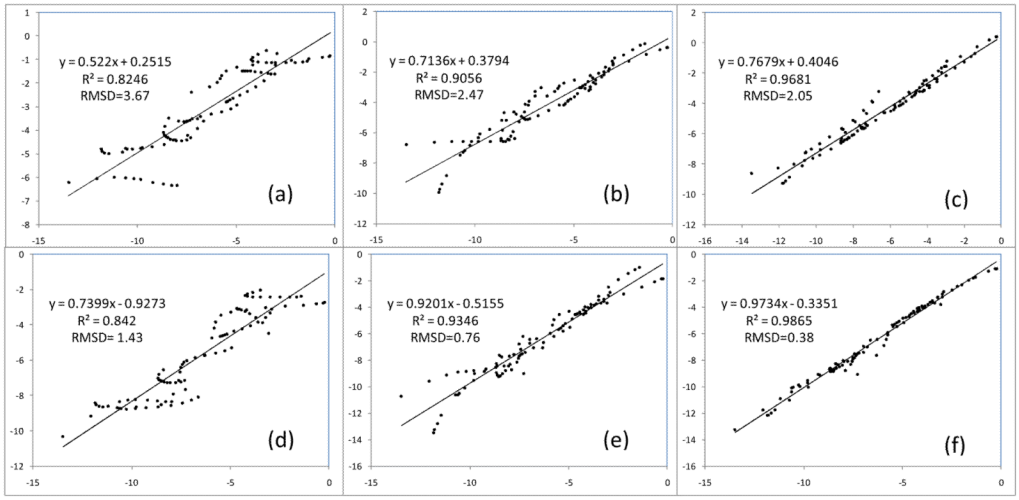

Figure 8.

Results of linear regressions of ΔE_{es} (in kcal/mol) between each electrostatic model and B3LYP-D3 DEDA results in describing HB directional dependence: (a) Atomic charge model; (b) Off-center point charge model; (c) Distributed multipole model; (d) Atomic smeared charge model; (e) Off-center smeared charge model; (f) Distributed multipole model with smeared charge. The x-axes correspond to the results from B3LYP-D3/aug-ccpvdz DEDA.

(A)

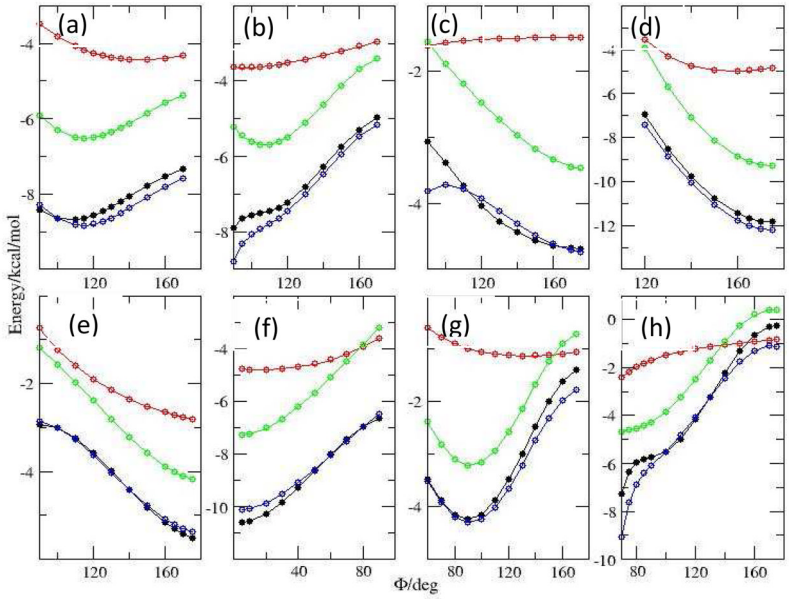

(B)

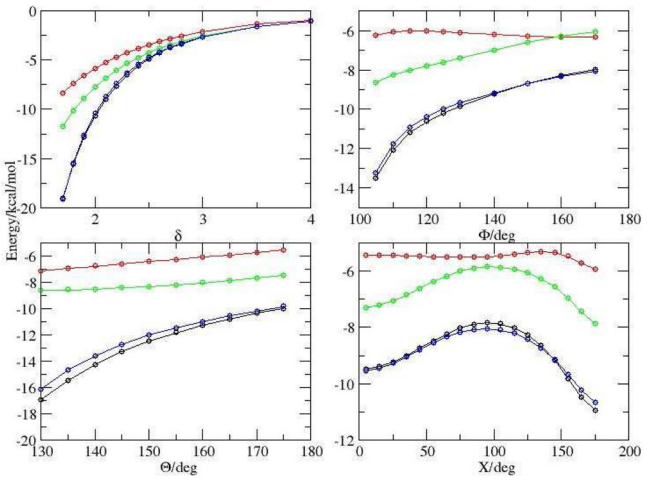

Figure 9.

ΔE_{es} (in kcal/mol) along the HB angles obtained from B3LYP-D3 DEDA and different electrostatic models. Black circle: DEDA; Red: atomic charge model; Green: distributed multipole model; Blue: distributed multipole model with smeared charge to take account of charge penetration effects. Other descriptions are the same as those in Figure 4.

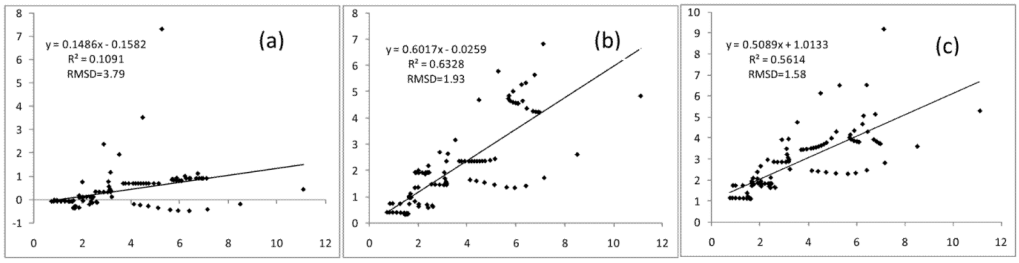

Figure 10.

Linear regression results for ΔE_{vdw} (in kcal/mol) between each vdW model and B3LYP-D3 DEDA. (a) LJ 12-6; (b) Buffered 14-7; (c) Buckingham. The x-axes correspond to the results from B3LYP-D3 DEDA.

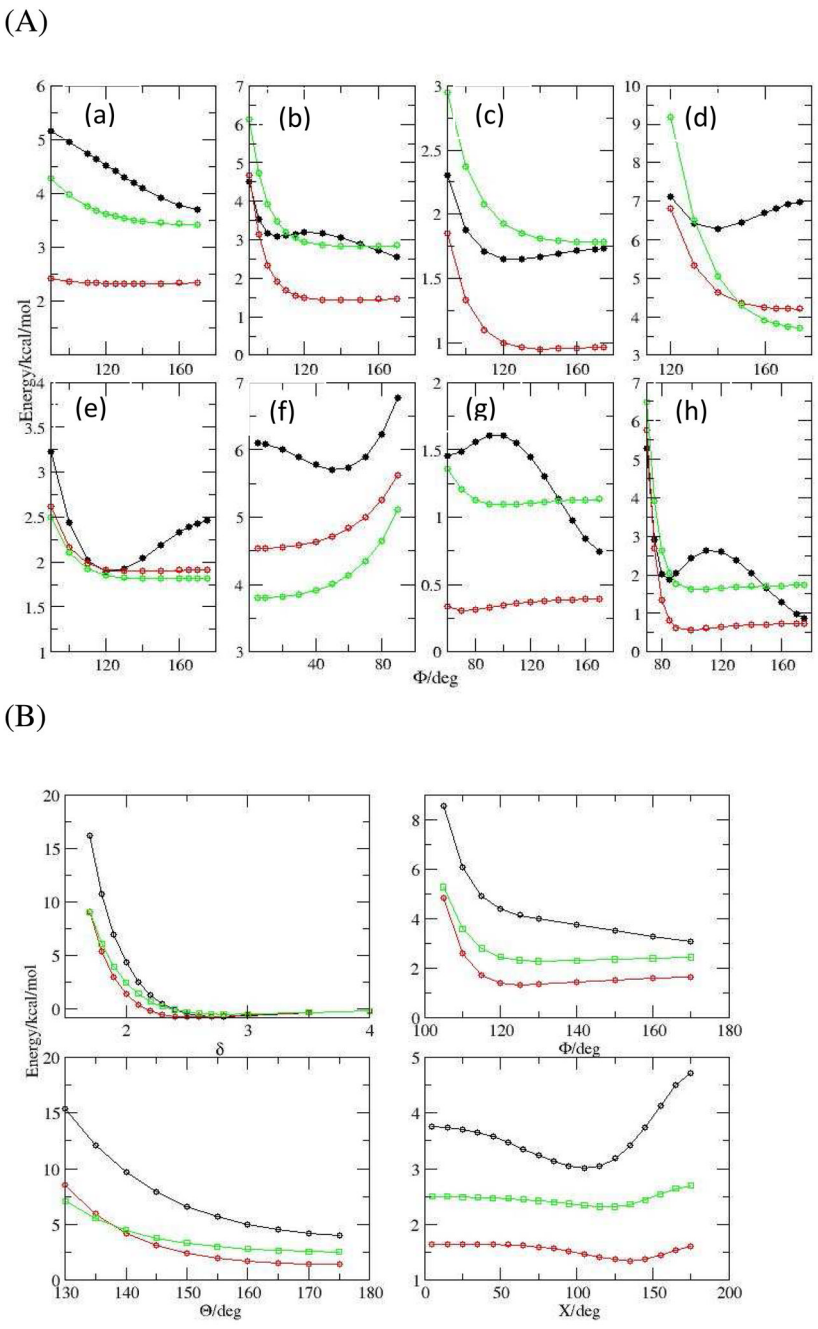

Figure 11.

vdW interactions along the HB angles obtained from B3LYP-D3 DEDA and various vdW models. Black: DEDA; Red: Buffered 14-7; Green: Buckingham. Other descriptions are the same as those in Figure 4.

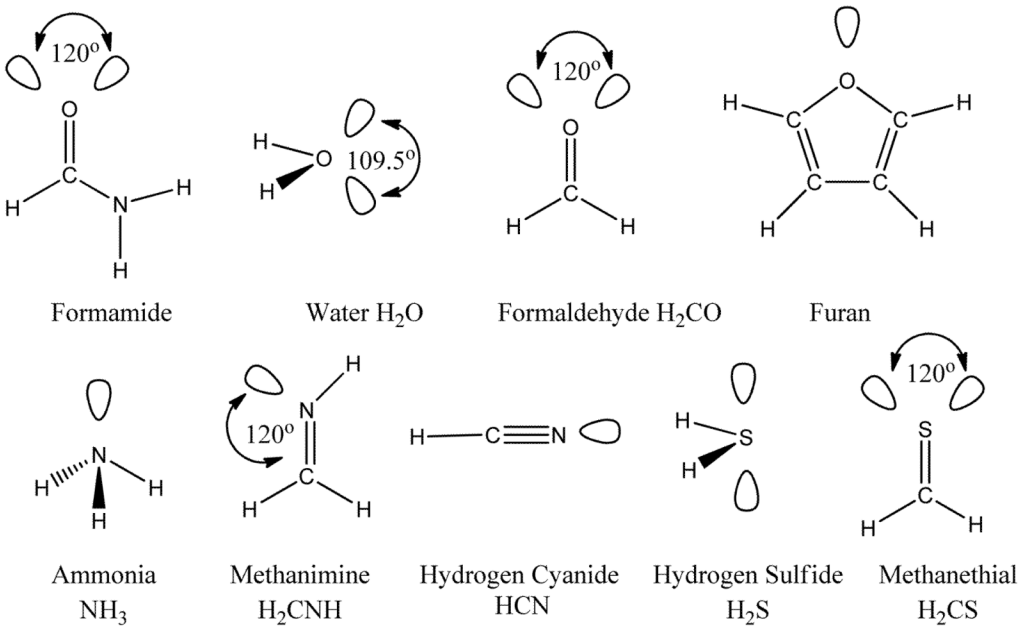

Scheme I.

Illustration of the placement of lone pairs on each molecule for the off-center charge model.

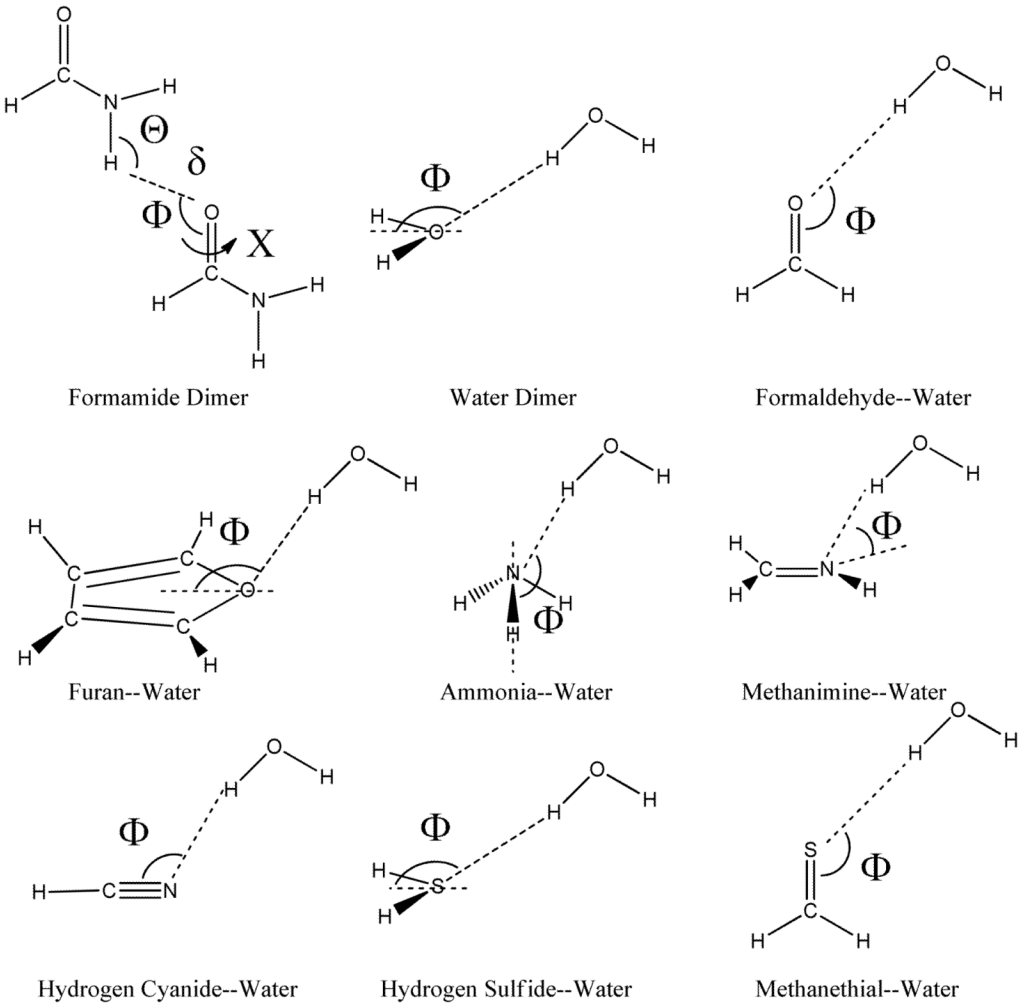

Scheme II.

HB complexes and the geometric HB parameters (denoted in Greek letters) used for EDA and model evaluations.

Table I

Percentage of energy components and total binding energy for each HB complex at geometries optimized at the B3LYP/aug-cc-pvdz level. ΔE_{frz}, ΔE_{pol}, and ΔE_{ct} are in percentage, and ΔE_{bind} is in kcal/mol.

	B3LYP-D3/aug-cc-pvdz				B3LYP-D3/aug-cc-pvtz				M06-2X-D3/aug-cc-pvdz			
	ΔE_{frz}	ΔE_{pol}	ΔE_{ct}	ΔE_{bind}	ΔE_{frz}	ΔE_{pol}	ΔE_{ct}	ΔE_{bind}	ΔE_{frz}	ΔE_{pol}	ΔE_{ct}	ΔE_{bind}
Water Dimer	79	9	12	−5.16	80	7	13	−5.24	79	11	10	−5.02
H_2CO–H_2O	83	7	9	−5.31	85	5	10	−5.38	84	8	8	−5.33
Furan– H_2O	83	4	13	−3.56	84	2	14	−3.63	81	7	12	−3.05
NH_3–H_2O	73	17	11	−6.73	75	14	11	−6.83	72	18	10	−6.37
HCN–H_2O	80	11	9	−3.80	82	7	11	−3.87	79	11	9	−3.57
H_2CNH–H_2O	76	13	11	−5.98	78	9	13	−6.07	75	14	11	−5.63
H_2S–H_2O	84	7	10	−3.16	84	3	13	−3.13	83	9	8	−2.95
H_2CS–H_2O	84	8	7	−4.67	85	7	8	−4.70	86	9	6	−4.86
Formamide Dimer	83	14	2	−7.55	85	13	2	−7.67	83	15	2	−7.46